Preferential Pathways for Fluid and Solutes in Heterogeneous Groundwater Systems: Self-Organization, Entropy, Work

1) Erwin Zehe, 1) Ralf Loritz, 2) Yaniv Edery, 3) Brian Berkowitz

1) Karlsruhe Institute of Technology (KIT), Institute of Water and River Basin Management, Karlsruhe, Germany; 2) Technion - Israel Institute of Technology, Haifa, Israel; 3) Department of Earth and Planetary Sciences, Weizmann Institute of Science, Rehovot, Israel

Corresponding author: Erwin Zehe (Erwin.Zehe@kit.edu)

Abstract

Patterns of distinct preferential pathways for fluid flow and solute transport are ubiquitous in heterogeneous, saturated and partially saturated porous media. Yet, the underlying reasons for their emergence, and their characterization and quantification, remain enigmatic. Here we analyze simulations of steady state fluid flow and solute transport in two-dimensional, heterogeneous saturated porous media with a relatively short correlation length. We demonstrate that the downstream concentration of solutes in preferential pathways implies a downstream declining entropy in the transverse distribution of solute transport pathways. This reflects the associated formation and downstream steepening of a concentration gradient transversal to the main flow direction. With an increasing variance of the hydraulic conductivity field, stronger transversal concentration gradients emerge, which is reflected in an even smaller entropy of the transversal distribution of transport pathways. By defining "self-organization" through a reduction in entropy (compared to its maximum), our findings suggest that a higher variance and thus randomness of the hydraulic conductivity coincides with stronger macroscale self-organization of transport pathways. Simulations at lower driving head differences revealed an even stronger self-organization with increasing variance. While these findings appear at first sight striking, they can be explained by recognizing that emergence of spatial self-organization requires, in light of the second law of thermodynamics, that work be performed to establish transversal concentration gradients. The emergence of steeper concentration gradients requires that even more work be performed, with an even higher energy input into an open system. Consistently, we find that the energy input necessary to sustain steady-state fluid flow and tracer transport grows with the variance of the hydraulic conductivity field as well. Solute particles prefer to move through pathways of very high power in the transversal flow component, and these pathways emerge in the vicinity of bottlenecks of low hydraulic conductivity. This is

because power depends on the squared spatial head gradient, which is in these simulations largest in regions of low hydraulic conductivity.

1 Introduction

1.1 Preferential flow phenomena – fast, furious and enigmatic

Distinct patterns of preferential movement of water, dissolved and suspended matter are ubiquitous in fully-saturated aquifer systems (e.g., LaBolle and Fogg, 2001; Bianchi et al., 2011; Berkowitz et al., 2006), partially saturated soils (e.g., Beven and Germann, 1982) and at the land surface (e.g., Howard, 1990). Preferential flow and solute transport in porous media commonly leads to fast, localized early arrivals and/or long tailing in temporal breakthrough curves (e.g., Berkowitz et al., 2006) and pronounced fingerprints in concentration patterns in soils (Flury et al., 1994).

Preferential flow and transport often occur along connected highly conductive networks of least flow resistance. Some networks are formed by previous physical/chemical work performed by the fluid, as in the cases of surface rill and river networks (Howard, 1990), subsurface pipe networks (Jackisch et al., 2017), karst conduits (Groves and Howard, 1994), and fractured rock formations (Becker and Shapiro, 2000; Berkowitz, 2002). Other networks are created by soil fauna and flora as earth worm burrows (Zehe and Flühler, 2001; van Schaik et al., 2014) and plant roots (Wienhöfer et al., 2009; Tietjen et al., 2009). Although it might appear unsurprising that flow and transport through these networks dominates system behavior, effective ways to model flow and transport in these networks have been debated for more than 30 years (Beven and Germann, 1981; Šimůnek et al., 2003; Klaus and Zehe, 2011; Wienhöfer and Zehe, 2014; Berkowitz et al., 2006, Sternagel et al., 2019, 2020). The emergence of preferential flow and transport in systems without well-defined networks – and their characterization – remains even more enigmatic (Bianchi et al., 2011; Edery et al. 2014). The numerical study of Edery et al. (2014), for example, revealed that a higher variance in the hydraulic conductivity (K) field coincided with a stronger concentration of solutes within a smaller number of preferential flow paths. If the emergence of preferential flow is indeed manifested self-organization, as argued by Berkowitz and Zehe (2020), this key finding of Edery et al. (2014) suggests that macroscale steady states of stronger organization (or higher order) emerge and persist despite a greater degree of randomness. The related key questions we address here are (i) how spatial

63 organization in preferential fluid flow and solute transport can be quantified, and (ii) why a
64 larger randomness might favor stronger macroscale organization.

65 **1.2 Attempts to characterize and predict preferential transport in groundwater**

66 The emergence of preferential pathways of fluid flow and solute transport in saturated porous
67 media has been explored in numerous simulation studies in heterogeneous conductivity fields,
68 to relate the spatial correlation structures of the hydraulic conductivity and velocity fields to
69 features of anomalous transport behavior (e.g., Cirpka and Kitanidis, 2000; Willmann et al.,
70 2008; Berkowitz and Scher, 2010; de Dreuzy et al., 2012; Morvillo et al., 2021). While velocity
71 correlation parameters have been successfully related to statistical moments of hydraulic
72 conductivity, it remains challenging to a priori delineate preferential pathways exclusively
73 based on multivariate and topological characteristics of the hydraulic conductivity field. Cirpka
74 and Kitanidis (2000) and Willmann et al. (2008) report, for instance, the emergence of
75 preferential pathways in the distributions of tracer travel velocities and shapes of solute plumes.
76 However, these pathways were not apparent from the analysis of the stationary conductivity
77 fields. Moreover, Edery et al. (2014) demonstrate that critical path analysis (based on
78 percolation theory), for example, does not determine the actual preferential pathways in a
79 system; the authors suggest that the operational preferential pathways become fully apparent
80 only when solving for fluid flow and solute transport through the domain.

81 Bianchi et al. (2011) explored the link between connectivity and the emergence of preferential
82 flow paths at the MADE site, using three-dimensional, conditional, geostatistical realizations
83 of the hydraulic conductivity field. Their simulations of flow and transport under permeameter-
84 like boundary revealed that the first 5% of particles, arriving at the downstream domain outlet,
85 moved through preferential flow paths carrying 40% of the flow. Fiori and Jankovic (2012)
86 reported similar findings and stressed the rather small probability that solute particles visit
87 highly conductive blocks particularly in case of a high variance in K. Bianchi et al. (2011)
88 highlighted that the fraction of particle paths passing the high-conductivity regions was between
89 43% and 69%, while the most rapid transport passed through low-conductivity bottle necks.
90 This is in line with the findings of Edery et al. (2014), who concluded that connectivity of rapid
91 preferential pathways need not require connected zones of continuously high hydraulic
92 conductivity. Along a different avenue, Bianchi and Pedretti (2017) characterized spatial
93 disorder in two-dimensional conductivity fields by means of the Shannon entropy (Shannon,

1948) and related this to moments of solute breakthrough curves. Dispersion in travel times and the probability of solutes to pass through high conductivity regions were found to increase with lower order expressed by a higher geological entropy.

1.3 Preferential flow, self-organization, entropy, work – where is the connection?

The results of all the studies mentioned above underpin that (a) preferential flow and transport in heterogeneous, saturated porous media remains a largely enigmatic phenomenon, and (b) there is no generalized framework allowing for predictions of this behavior by means of effective transfer functions, which are inferred from volume-averaging based scaling of the hydraulic conductivity field. This is why, we propose to shift the attention from the question of "where" preferential pathways emerge, to questions regarding their "macroscale organization and strength", and "the necessary physical work" to establish their self-organized emergence.

Haken (1983) defined self-organization as the emergence of ordered macroscale states, or the dynamic behavior of an open system far from thermodynamic equilibrium (TE), that arises from a synergetic interplay of microscale, irreversible processes. An ordered state is characterized by the deviation of its entropy from the entropy maximum at TE (Kondepudi and Prigogine, 1998). This reduction in entropy, and any additional entropy produced by the internal irreversible processes, must be exported from the open system to establish order. This is turn requires physical work, and thus an input of free energy into the system, that is large enough to create and maintain the self-organized state. A classical example to illustrate that self-organization in open systems requires free energy and work, which inspired also Haken's theory of "synergetics", is a gas laser. Laser light results from coherent stimulated light emissions from all molecules in the system. Stimulated emission emerges when the energy input into the gas laser becomes sufficiently large that the number of stimulated molecules exceeds the number of molecules in the basic state. This "energetic pumping" establishes a state very far from thermodynamic equilibrium, corresponding even to an apparently negative absolute temperature in Boltzmann statistics, at which coherent emission from all individual emissions emerges. Haken (1983) postulated that a higher-order, non-local "enslavement principle" forces the individual molecules into a coherent and thus ordered behavior. This example of a critical pumping rate to establish organization of laser light will be shown below to be analogous to fluid flow through porous media.

Several researchers have suggested that self-organization and the formation of complex organisms and patterns in biological and environmental systems are governed by non-local/global energetic extremal principles, in analogy to the Haken (1983) enslavement principle. Pioneering studies in this context proposed that species maximize their energy throughput (i.e., power) during evolution (Lotka, 1922 a &b) or showed that steady-state planetary heat transport may be modeled successfully with a very simple two-box model, when assuming that this state maximizes entropy production (Paltridge, 1979). This work motivated several studies that explored the possibility that energetically optimized model setups allow hydrological prediction of the land surface energy balance and evaporation (Kleidon et al., 2014), rainfall runoff behavior (Zehe et al., 2013) and groundwater flow and spring discharge (Hergarten et al., 2014). These and other studies generally showed that preferential flow in connected networks allows for a more energy efficient throughput of water and matter through the system. This is because they reduce flow-weighted dissipative losses due to an increased hydraulic radius in the rill or river network compared to sheet overland flow (Howard, 1990; Kleidon et al., 2013) or in subsurface connected preferential pathways compared to matrix flow (Hergarten et al., 2014; Zehe et al., 2010).

While the second law of thermodynamic refers to physical entropy (introduced by Clausius (1857)), Sect. 3.1), information entropy (introduced by Shannon (1948)) is closely related and well suited for diagnosing spatial organization (see Sect. 3.3). The concepts of information and Shannon entropy have been widely used to characterize irreversible mixing and reaction processes and their predictability (Chiogna and Rolle, 2017), the emergence of order in distributed time series (Mälicke et al., 2020), information in multiscale permeability data (Dell`Oca et al., 2020) and the role of spatial variability of rainfall and topography in distributed hydrological modelling (Loritz et al., 2018, 2021). Woodbury and Ulrych (1993) and Kitanidis (1994) used the Shannon entropy to describe the spatial-time development and dilution of tracer plumes in groundwater systems. Chiogna and Rolle (2017) expanded the dilution index for the case of reactive solute mixing in groundwater and found a critical value that indicated the complete consumption of a reactant, which was independent of advection and dispersion. Bianchi and Pedretti (2017) used the Shannon entropy to quantify spatial disorder in stochastically generated alluvial aquifers and explored its relation to the first three moments of simulated tracer break through curves. They found the average breakthrough time and its variance to increase with increasing geological entropy, while the skewness in travel times

declined with increasing geological entropy and thus increasing disorder. In a follow up study, Bianchi and Pedretti (2018) generalized their local geological entropy concept to multiple block sizes. The resulting entrogram quantifies how local entropy of, e.g., hydraulic conductivity in a block converges to the entropy in the entire domain when subsequently increasing the block size. While the entrogram appears similar to a variogram, the related entropic length scale is helpful to explain the various characteristics of simulated breakthrough curves in multivariate Gaussian and non Gaussian media.

1.4 Objectives

We thus suggest that the concepts of entropy, free energy and work hold the key to better understand why preferential flow and transport in unstructured heterogeneous, saturated porous media actually emerge. To this end, we analyze simulations of fluid flow and solute transport through stochastically heterogeneous aquifers with different degrees of randomness (variance in hydraulic conductivity), based on the results and insights of Edery et al. (2014). We propose that macroscale self-organization due to the downstream emergence of preferential solute transport can be quantified based on the downstream decline of the Shannon entropy of the transversal concentration pattern. We propose, furthermore, that the concentration of solutes into a smaller number of preferential paths, as observed by Edery et al. (2014) in the case of higher variances in hydraulic conductivity, coincides with a state of stronger self-organization/ and thus a lower entropy. Finally, we propose that this apparent paradox – in the sense that a higher randomness of the medium hydraulic conductivity causes a stronger spatial organization of pathways – can be explained by comparing power in fluid flow and the related work performed by the fluid among the different media and driving head differences.

2 Underlying simulations of fluid flow and transport

2.1 Media generation and numerical simulations of fluid flow

Before we detail the concepts of free energy, entropy and work in Sect. 3, we revisit and expand upon the numerical simulations of Edery et al. (2014), because they form the main motivation of this study. Edery et al. (2014) considered steady-state fluid flow within a two-dimensional, stochastic heterogeneous system. The flow domain measured 300 by 120 space units as discretized into grid cells of uniform size $\Delta x = 0.2$, $\Delta y = 0.2$, while all quantities that relate to these simulations are expressed using the same space-time units. In a first attempt, we consider

a deterministic head difference of $\Delta H = 100$, from the left (vertical) upstream boundary to the right downstream boundary as well as additional simulations with a head difference of $\Delta H = 10$ across the domain; while no-flow conditions are assigned to the two horizontal domain boundaries.

We generated random realizations of statistically homogeneous, isotropic Gaussian fields for the natural logarithm of the hydraulic conductivity $\ln(K)$, with exponential covariance and mean $\ln(K) = 0$, using the sequential Gaussian simulator GCOSIM3D (Gómez-Hernánez et al,. 1997). Edery et al. (2014) considered fields associated with a unit correlation length for the covariance function, $l = 1$, exploring the impact of different values of the variance of $\ln(K)$, i.e., $1 < \sigma^2 < 5$, on the emergence of preferential solute transport.

Figure 1a, b and c show single realizations for $\sigma^2 = 1$, 3, and 5, corresponding to mild, intermediate and strong randomness, respectively. The deterministic flow problem for each realization was solved using a code that is based on finite elements with Galerkin weighting functions (Guadagnini and Neuman, 1999). The corresponding hydraulic head values throughout the domain were converted to local velocities, and thus streamlines (Fig. 1b), which were in turn used for transport simulations using particle tracking. For the system considered here, we used a porosity of 0.3 (e.g., Levy and Berkowitz, 2003).

2.2 Simulated solute transport with particle tracking and emergent preferential transport

Solute movement in each domain realization and for the two head differences was simulated using the calculated streamlines, with a standard Lagrangian particle tracking method. The head differences correspond to Peclet numbers of Pe = 597and 59.7representing a relative importance of advective transport against diffusion ranging from strong to intermediate dominance. For all domains, values of Δ and l were chosen such that $l/\Delta = 5$, to enable capture of small-scale fluctuations and advective transport features (Ababou et al., 1989; Riva et al., 2009). Along the left upstream boundary, particles are injected, by flux-weighting, and advance by advection and diffusion. The Langevin equation defines the particle displacement vector $\mathbf{r}$, starting from given particle locations at time t_k:

$$\mathbf{r} = \boldsymbol{v}[\mathbf{x}(t_k)]\delta t + \boldsymbol{d}_o \quad \text{(Eq. 1)}$$

where $\boldsymbol{v}$ is the fluid velocity vector, δt is the time step magnitude, and $\boldsymbol{d}_o$ denotes the diffusive displacement, with a modulus of $\boldsymbol{d}_o$ given by $\xi\sqrt{2D_{\mathrm{mol}}\delta t}$; ξ is a random number drawn the from standard normal distribution $N[0, 1]$. A representative molecular diffusion coefficient of $D_{\mathrm{mol}} = 10^{-9}$ m^{2}s^{-1} was prescribed (Domenico and Schwartz, 1990). The advective displacements in Equation 1 are computed using the local velocities at **x** with a fixed, uniform spatial step δs. In Equation 1, the time step δt is given by $\delta t = \delta s/v$, where v is the modulus of $\boldsymbol{v}$. Reflection conditions are prescribed along the two horizontal no-flow boundaries to avoid particle leakage. As in Edery et al. (2014), we used 10^5 particles, with $\delta s = \Delta/10$.

As explanation of the formation of preferential transport patterns is the main motivation of the thermodynamic framework we present in Sect. 3, we briefly compare these patterns for a randomly selected realization as a function of the variance, σ^2, for the head difference ΔH = 100 (Fig. 1d – f) and 10 (Fig. 1g – i), respectively.

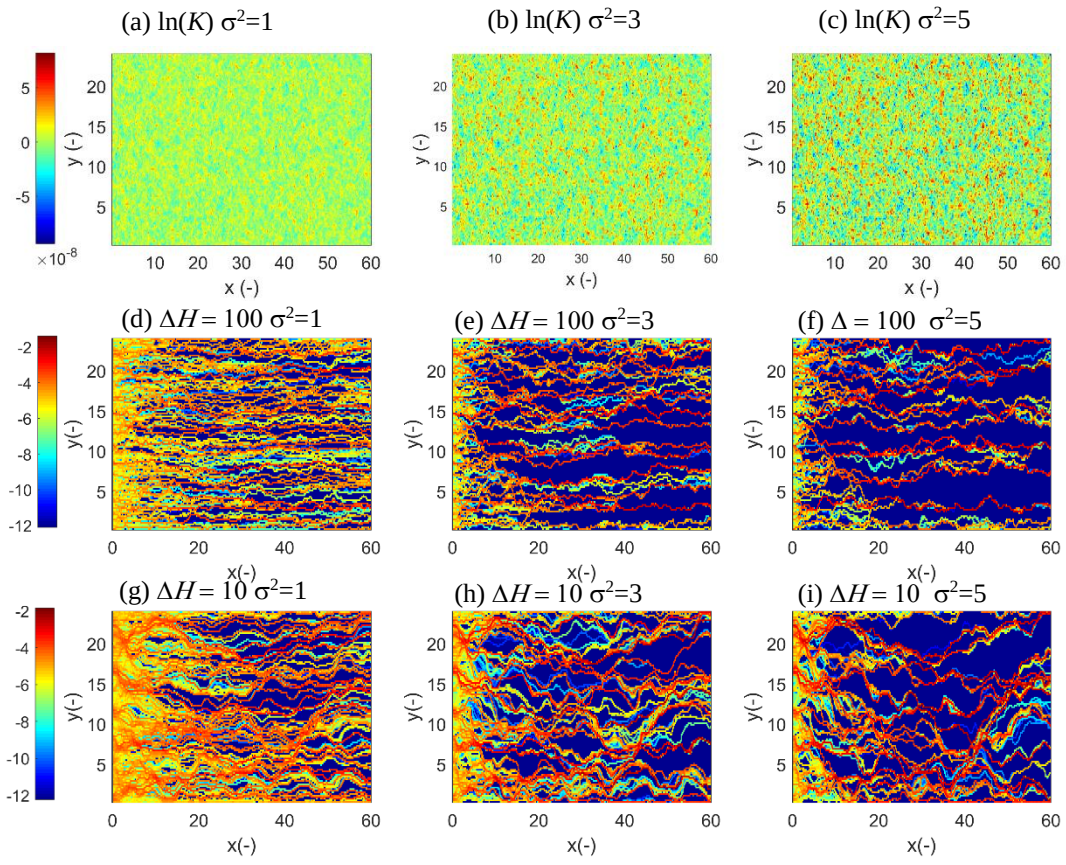

Figure 1. Examples of **(a-c)** ln(K) for variances σ^2 = 1, 3 and 5, respectively, and the corresponding cumulative number of particles that visited a grid cell in the simulation domain normalized with the total number of N particles, for the head differences **(d-f)** ΔH = 100 and **(g-i)** 10. This corresponds to Peclet numbers of 597 and 59.7, respectively.

For the head difference ΔH = 100, transport pathways, visualized by the accumulated particle densities that passed through the grid cells, extend in a largely parallel form and share rather similar particle densities for σ^2=1 (Fig. 1d). However, the number of preferential pathways clearly declines with increasing variance, and they exhibit a stronger meandering on their downstream course (Fig. 1e, f). Transport pathways in case of the 10 times smaller head gradient evolve in a qualitatively similar fashion, with a stronger downstream concentration of particles into a smaller number of preferential pathways when moving to larger variances. However, the meandering of preferential channels is more distinct. As already stated, Edery et al. (2014) performed a critical path analysis to examine the formation of preferential pathways, based on the common assumption that preferential flows are a manifestation of percolation, controlled by the lower cut-off for the hydraulic conductivity from which a path is possible. This analysis revealed that percolation considerations are not relevant for explaining these differences in preferential flow and transport behavior, as the domains are well connected and well above a percolation threshold.

3 Free energy, entropy and work

3.1 Thermodynamics in a nutshell: the first and the second law

We start very generally with the first law of thermodynamics, which relates the variation in internal energy U (J = kg m^2 s^{-2}) of a system to a variation of work E_{free} (J) and a variation of heat Q_h (J), while overall energy is conserved:

$$\delta U = \delta E_{free} + \delta Q_h \ (Eq. 2)$$

Note that the capacity of a system to perform work is equivalent to "free energy", while a variation in heat is equal to the product of a variation of physical entropy S (J K^{-1}) and the absolute temperature T (K): $\delta Q_h = T\ \delta S$ as introduced by Clausius (1857). The second law of thermodynamics states that entropy is produced during irreversible processes, while it cannot be consumed. The second law implies that isolated systems, which neither exchange mass, nor energy, nor entropy with their environment, reach a dead state of maximum entropy called thermodynamic equilibrium in which all gradients have been depleted. Kleidon (2016) distinguishes three types of physical entropy: thermal entropy produced by friction and depletion of temperature gradients, molar entropy produced by mixing and depletion of

chemical potential/concentration gradients, and radiation entropy produced by radiative cooling and depletion of radiation temperature differences.

From Eq. 2 and the second law, we can conclude that free energy is not a conserved property, as it corresponds to the variation in internal energy minus the variation in heat, during which entropy is produced. Free energy dissipation and entropy production are thus inseparable, and maximization of the entropy of an isolated system occurs due to conservation of energy at the expense of minimizing its free energy. An open system may nevertheless persist in steady states of lower entropy, if it is exposed to a sufficient influx of free energy to sustain the necessary physical work that needs to be performed to act against the natural depletion of the internal gradients, or even to steepen them and further reduce the entropy (as discussed for the gas laser). Order in an open system thus manifests through persistent gradients and an entropy lower than the maximum. Steps to higher order and lower entropies imply a steepening of internal gradients. This is exactly what occurs when preferential transport of solutes emerges in our transport simulations: solute particles tend to concentrate in localized pathways, thereby forming a transversal concentration gradient (according to the domain geometry shown in Fig. 1). The Shannon entropy (Shannon, 1948) is ideally suited to quantify the related entropy reduction, as detailed in Sect. 3.3.

3.2 The free energy balance of saturated porous media

To determine the work that is performed by the fluid when flowing through heterogeneous media, we derive the free energy balance of the fluid by relating changes in hydraulic head and fluid flux to their energetic counterparts. The local formulation of the free energy balance of a groundwater system, seen as an open thermodynamic system, is determined by the difference/divergence of the free energy fluxes $\boldsymbol{J}^{E}_{free}$ (J s^{-1} m^{-2}) per unit area and the amount of dissipated energy per volume D (J s^{-1} m^{-3}):

$$\frac{\partial e_{free}}{\partial t} = -\nabla \cdot \boldsymbol{J}^{E}_{free} - D \quad \text{(Eq. 3)}$$

where e_{free} (J s^{-1} m^{-3}) is the volumetric free energy density. Advective fluxes of relevant free energy forms are generally determined by multiplying the Darcy flux with the corresponding form of energy per unit volume. Here we account for advection of mechanical energy $\boldsymbol{J}^{E}_{H}$ (named power hereafter), gravitational potential energy $\boldsymbol{J}^{E}_{pot}$, and kinetic energy of the flowing

fluid $\boldsymbol{J}^{E}_{kin}$. As energy is additive, the term $\boldsymbol{J}^{E}_{free}$ corresponds hence to the sum of the following free energy fluxes:

$$\boldsymbol{J}^{E}_{H} = \boldsymbol{q}\rho g H$$

$$\boldsymbol{J}^{E}_{pot} = \boldsymbol{q}\rho g z \ (Eq.\,4)$$

$$\boldsymbol{J}^{E}_{kin} = \boldsymbol{q}\frac{1}{2}\rho v^{2}$$

where ρ (kg m^{-3}) is the density of water, g (m s^{-2}) the gravitational acceleration, $\boldsymbol{q}$ (m s^{-1}) the Darcy flux vector, v (m s^{-1}) the absolute value of the fluid velocity, H (m) the pressure head, and z (m) the geodetic elevation. Note that while kinetic energy is proportional to v^2, the kinetic energy flux corresponds to the product of the volumetric water flux $\boldsymbol{q}$ and its kinetic energy density ½ ρv^2. Thus, kinetic energy is in fact proportional to v^3 and is usually very small. By inserting Eq. 4 into Eq. 3 and assuming a constant fluid density, we obtain:

$$\frac{\partial e_{free}}{\partial t} = -\rho g \nabla \cdot [\boldsymbol{q}(H+z)] - \frac{1}{2}\rho \nabla \cdot [\boldsymbol{q}v^{2}] - D \ (Eq.\,5)$$

The left hand side of Eq. 5 corresponds to the change in Gibbs free energy of a fluid volume under isothermal conditions (Bolt and Frissel, 1960). This change in free energy storage on the left hand side can be decomposed into the sum of three terms as well (Zehe et al., 2019): (i) the change in storage of gravitational potential energy reflecting soil water storage changes in partially saturated soils or density changes in groundwater; (ii) the change in storage of mechanical energy reflecting changes in pressure head in groundwater or changing matric potentials in partially saturated soils; and (iii) the change in kinetic energy stored in the system, due to acceleration of the fluid. The latter is usually very small and can be neglected.

In the case of steady-state conditions, the change in free energy storage at the left hand side of Eq. 5 is zero. As z is constant along the system and we neglect density changes of the fluid, the divergence in the flux of gravitational potential energy at the right hand side is zero, as well. The system under investigation hence receives solely steady-state inflow of high mechanical energy, corresponding to the upstream inflow of water at a high pressure head, and it exports water with a much lower mechanical energy at the lower downstream pressure head. The corresponding energy difference is partly dissipated and partly converted into kinetic energy of flowing fluid and dissolved solute masses. The latter is, however, usually neglected, as

dissolved solute mass is much smaller. As steady-state fluid flow further implies that the divergence of $\boldsymbol{q}$ is zero as well, the free energy (Eq. 5) becomes hence:

$$\rho g \boldsymbol{q} \cdot \nabla H = -\rho v \boldsymbol{q} \cdot \nabla v - D \ (Eq. 6).$$

The left hand side is the available power per unit volume P (J s^{-1} m^{-3}) in the groundwater flux, which is partly converted into a spatial change in kinetic energy of the fluid and partly dissipated. In contrast to overland flow systems (Loritz et al., 2019; Schroers et al., 2021), the change in kinetic energy can be neglected for groundwater as it is proportional to the cube of the fluid velocity (as noted before Eq. 5). In fact, the use of Darcy's law implies that kinetic energy can be neglected.

The total available power P in the groundwater flux during steady-state flow is hence nearly completely dissipated:

$$P = \rho g \boldsymbol{q} \cdot \nabla H = -D \ (Eq. 7).$$

By inserting Darcy's law into Eq. 7 and recalling that we focus on a two-dimensional domain, we obtain an equation that relates power and dissipation to the squared head gradient (in sense of a scalar product):

$$P = -\rho g K \left[\frac{\partial H}{\partial x}\frac{\partial H}{\partial x} + \frac{\partial H}{\partial y}\frac{\partial H}{\partial y}\right] = -D \ (Eq. 8).$$

The physical mechanism that causes dissipation relates to the shear and frictional losses the fluid experiences when passing through the porous medium. As hydraulic conductivity relates to the ratio of intrinsic permeability k (m^2) and viscosity of the fluid η (N sm^{-1}), the inverse of K is a measure of the flow resistance and related dissipative losses. One would thus expect that the dissipative losses grow with fluid viscosity (declining K, increasing resistance) and declining permeability (declining k). To better underpin this, we simplify Eq. 8 for steady-state flow through an heterogeneous, one-dimensional system, which means that $\frac{\partial H}{\partial y}$=0:

$$P = \rho g (K(x) \mathrm{d}_x H) \mathrm{d}_x H = D(x) \ (Eq. 9).$$

where d_x denotes the gradient with respect to x. Steady-state flow in one dimension implies a constant flux q in the x direction, which means that the total spatial variation of dq is zero. As K is spatially variable, this implies that local spatial variations of conductivity denoted by

345 $d_x(K(x))$ must be compensated by opposite spatial variations of the pressure head gradient,
346 $d_x(d_xH)$:

347 $$d_x q = 0 \rightarrow$$

348 $$d_x(-K(x)d_xH) = 0 \rightarrow$$

349 $$-d_x\big(K(x)\big)\, d_xH = K(x)\, d_x(d_xH) \quad Eq.(10)$$

350 As a consequence, power P is not constant (Eq. 7) but instead grows with the magnitude of
351 local spatial variations of the head gradient $d(\nabla_x H)$:

352 $$d_xP = \rho g q\, d_x(d_xH)\ (Eq.11).$$

353 Due to Eq. 10 (constant Darcy flux), we can express the spatial variation in the head gradient
354 $d_x(d_xH)$ in Eq. 11 as follows:

355 $$-d_xH\, d_x\big(\ln\big(K(x)\big) = d_x(d_xH\big) \qquad (Eq.12).$$

356 Combining Eq. 12 with Eq. 11, together with the definition of power in Eq. 9, yields:

357 $$d_xP = -P(x)\, d_x\big(\ln\big(K(x)\big) \rightarrow d_x(\ln(P(x)\big) = -d_x(\ln\big(K(x)\big)\ (Eq.13).$$

358 As a consequence, we expect an anti-proportionality between $\ln(P(x))$ and $\ln(K(x))$ for the one-
359 dimensional case. In conclusion, we propose that the necessary power to push the fluid through
360 an heterogeneous medium grows also in the two-dimensional case with the variance of the $\ln(K)$
361 field. Local areas of high power coincide with large positive deviations from the overall average
362 head gradient, and these in turn peak across regions of low conductivity. This makes sense, as
363 dissipation peaks in those areas as flow resistance reach a maximum and the required work to
364 push fluid through these bottlenecks grows as well. This potentially explains the finding of
365 Edery et al. (2014) that the preferential flow paths also pass through areas of low conductivity.
366 We discuss this idea further in Sect. 5.

367 **3.3 Characterizing emergent spatial organization in solute transport using information**
368 **entropy**

369 **3.3.1 Information entropy and its relation to physical entropy**

370 We now address the connection between physical entropy and information entropy, and explain

how we use the latter to quantify ordered states due to the emergence of preferential flow paths and the associated formation of a concentration gradient transversal to the main flow direction. The Shannon entropy S_H (bit) is defined as the expected value of information (Shannon, 1948). Here we defined S_H using the discrete probability distribution to find particles at a distinct transversal position y at a given x coordinate, as detailed below.

The field of information theory, originally developed within the context of communication engineering, deals with the quantification of information with respect to a concept called *"*surprise" of an event (Applebaum, 1996). For a discrete random variable Y that can take on several values y_i with associated prior probabilities $p(y_i)$ the surprise or information content of receiving/observing a specific value $Y = y_i$ is defined as:

$$I = -\log_b\big(p(y_i)\big) \quad \text{(Eq. 14)}$$

where I is the information content, b is the base of the logarithm and $p(y_i)$ the prior probability that Y can be observed in the state y. Due to the use of the logarithm in Eq. 14, information is an additive quantity, similar to physical entropy, energy, and mass. The expected information content associated with the probability distribution of the random variable Y is the Shannon entropy S_H:

$$S_H(Y) = -\sum_{y \in Y} p(y_i)\, log_2\ p(y_i) \quad \text{(Eq. 15)}$$

The definition of the Shannon entropy is equivalent to Gibb's definition of physical entropy in statistical mechanics (Ben-Naim, 2008). The latter is obtained when using the natural logarithm in Eq. 15 and by multiplying the sum with the Boltzmann constant (k_B=1.30640 × 10^{-23} J K^{-1}). Physical entropy describes, in terms of statistical mechanics, the number of microstates that correspond to the same macro-state at a given internal energy. In the state of maximum entropy where all gradients are depleted, each microstate is equally likely (Kondepudi and Prigogine, 1998). The probability p of a single state is in this case, hence, simply the inverse of the number of microstates. This implies a maximum uncertainty about the microstates and corresponds to a minimum order in the system. Jaynes (1957) transferred this fundamental insight into a method of statistical inference, stating *"when making inferences based on incomplete information, the best estimate for the probabilities is the distribution that is consistent with all information, but maximizes uncertainty*". We emphasize that a maximum in information

entropy and physical entropy commonly implies a zero gradient either in probability (from the information perspective) or in an intensive state variable such temperature, concentration or pressure (from the thermodynamic perspective).

3.3.2 Calculation of flow path entropy in concentration patterns

Its straightforward implementation makes the Shannon entropy a flexible means (i) for the optimization of observation networks (Fahle et al., 2015; Nowak et al., 2012), (ii) for the characterization of mixing and dilution of solute plumes (e.g., Woodbury and Ulrych, 1993; Kitanidis, 1994), or (iii) to illuminate how spatial disorder in hydraulic conductivity relates to statistical moments of solute breakthrough curves (Bianchi and Pedretti, 2017). Here we adopt a straightforward use of the Shannon entropy to characterize simulated solute transport, as introduced by Loritz et al. (2018) to characterize redundancy in a distributed hydrological model ensemble. We suggest that the maximum uncertainty corresponds to the case where each flow path through the domain is equally likely, and the probability distribution to find particles in a position in the *y*-direction is, hence, uniform. Deviations from this entropy maximum reflect spatial order due to the concentration of particles in preferred flow paths and the associated persistence of a transversal concentration gradient. This can be analyzed by computing the Shannon entropy of the particle density distributions along *y*, $S_H(x)$, at a fixed position *x* along the main flow direction, using the particle density matrix. A state of maximum entropy implies that the same number of particles has visited each of the 120 grid cells at a given *x* coordinate i.e. $S_H^{max} = log_2\,(120) = 6.9$ bits. A state of perfect spatial organization and zero entropy arises, on the other hand, when all particles move through a single grid cell at a distinct coordinate *x*.

4 Results

In the following, we present the Shannon entropy of transversal flow paths distribution and relate this to power in the fluid flow across the range of the variances in ln(*K*) and head differences, respectively. For this purpose, we set the dimensionless length and time units to meters and seconds, respectively.

4.1 Preferential flow paths and flow path entropy as function of the variance in ln(*K*)

Figures 2a-c compare the accumulated particle densities that passed through grid cells in the domain as a function of the variance, σ^2, for a randomly selected realization, for the head difference of 100 m. The solute transport pathways extend in a largely parallel form and share rather similar particle densities for σ^2=1. However, the number of pathways clearly declines with increasing variance, and they exhibit a stronger meandering and a larger visitation of particles in a smaller transversal number of grids on their downstream course. The Shannon entropy S_H of the flow paths (flow path entropy hereafter) exhibits, in general, and for all three variance cases, a clear decline with increasing downstream transport distance (Figs. 2d-f).

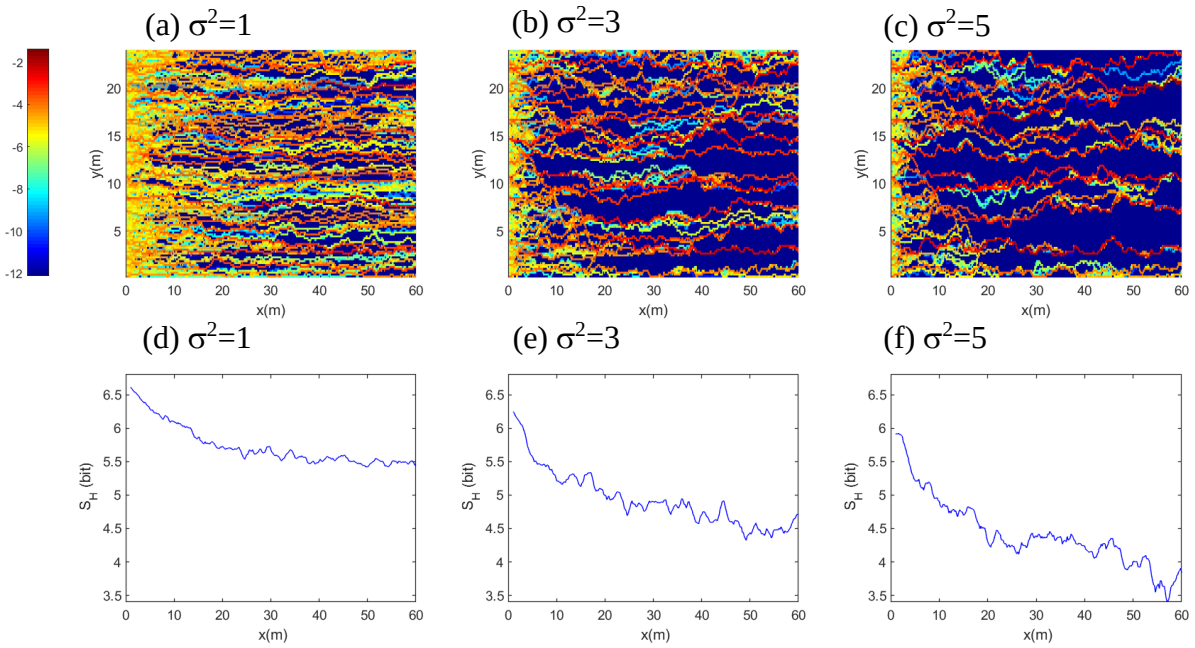

Figure 2. Accumulated, normalized number of particles that passed a distinct point in the domain as function of the variance in ln(*K*), σ^2, (**(a)**, **(b)**, **(c)**) and the corresponding Shannon entropy of the transversal concentration, $S_{H,}$ as a function of the main flow direction (**(d)**, **(e)**, **(f)**).

This reflects the increasing order in the flow path distribution, corresponding to the emerging and increasing transversal concentration gradients. A comparison of S_H among the variance cases clearly corroborates the visual impression that the number preferential flow paths declines with increasing randomness, while the concentration of solutes therein increases. The analysis of flow path entropy within the entire set of 100 realizations revealed that this behavior is not an artefact of single realization. The flow path entropy averaged across all realizations of a variance case exhibits a steady downstream decline (Fig. 3a, ΔH = 100 m). The curves are

clearly shifted to lower values with increasing variance of ln(K), and the differences between the averages exceed the standard deviations within the ensembles. The boxplots in Fig. 3b (ΔH = 100 m) characterize the distribution of $S_H(x)$ at the downstream outlet among the realizations. While the spreading and the skewness of the distribution clearly increases with increasing variance in ln(K), we also observe that flow path entropy at the outlet declines clearly and statistically significantly with increasing variance, as the differences between the medians exceed the confidence limits.

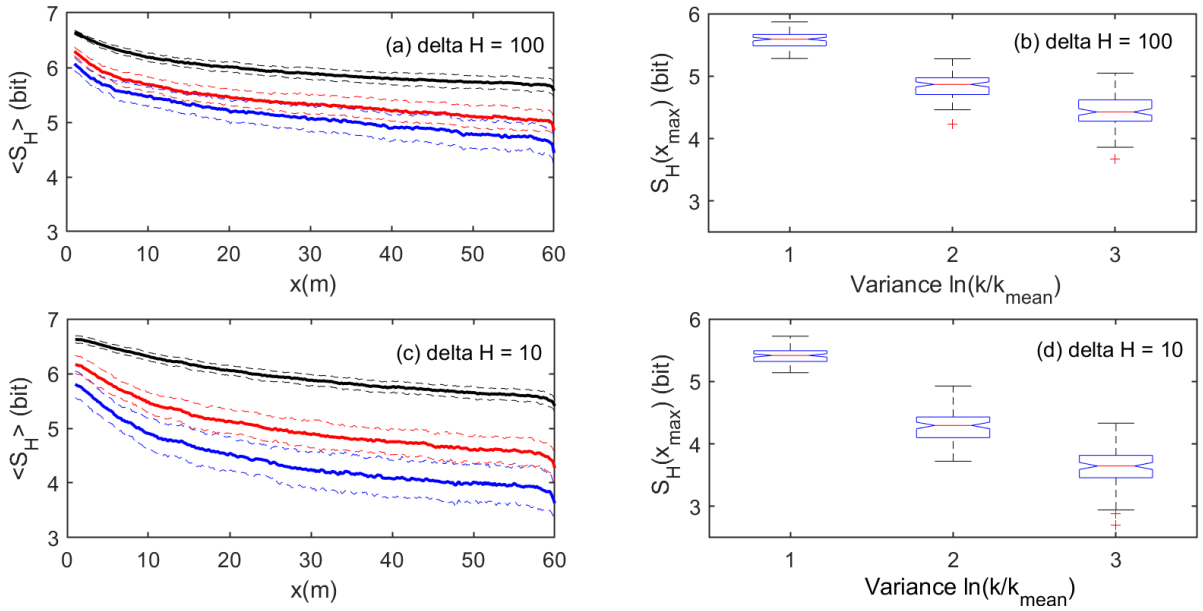

Figure 3. Flow path entropy averaged across all 100 ensemble realizations <S_H> as function of downstream transport distance for **(a)** ΔH = 100 m, and **(b)** ΔH = 10 m; the dashed lines mark the range plus/minus the standard deviations. Boxplot of flow path entropy at the domain outlet for all realizations of the three variance cases for **(c)** ΔH = 100 m, and **(d)** ΔH = 10 m; note this corresponds to the asymptotic values in (a) at x = 60 m.

We thus state that a higher variance – and thus randomness – in hydraulic conductivity coincides, for all realizations, with stronger a downstream reduction of the flow path entropy. This corresponds to a macrostate of higher order due to a more efficient self-organization into a state of stronger preferential transport. In case of the lower driving head difference of ΔH = 10 m, an even stronger self-organization manifests, as reflected in the smaller average flow path entropies for variances of σ^2 = 3 and 5, respectively (Fig. 3c and d).

4.2 Power in fluid flow as function of the variance in ln(K)

Figures 4a-c compare the distribution of power in the fluid flow calculated according to Eq. 7, as a function of the variance of ln(K) in the different domains for the driving head difference of ΔH = 100 m. For consistency, we used the same ensemble as for Fig. 2. The distributions of power in the fluid generally spread across a wide range of magnitudes and are skewed to the left. However, the distributions clearly shift to larger values and their spread becomes wider when moving to larger variances. This is underpinned when comparing the integrated power in fluid flow across the entire two-dimensional domain. An increase in variance by two orders of magnitude in the log-normal scale corresponds to an increase in power of 2.28 W per unit width of the domain. A closer look reveals that this increase in total power stems mainly from the increasing power in the vertical/transversal flow component (Fig. 4d-f). To further illuminate whether the above postulate of a strong linear relation between power and variation in the head gradient exists, we integrated power in fluid flow across the transversal extent of the domain (P^x_{int} hereafter) and plotted it against the laterally averaged head gradient (Fig. 3g-i). In the case of a unit variance, this indeed yields a strongly linear relation, with an almost perfectly linear growth of P^x_{int} with the head gradient, as indicated by the correlation coefficient of 0.96. While this the correlation becomes weaker with increasing variance, it remains significant even for the case of $\sigma^2 = 5$ with a correlation coefficient of $r = 0.84$. The decline in correlation is plausible as a higher variability in K in the two-dimensional domains, causes stronger transversal flow components and thus a larger deviation from the one-dimensional heterogeneous case for which Eqs. 9-12 are valid. The increasing role of transversal flow is also reflected by the increasing power in the vertical flow component with increasing variance (Fig. 4d-f). As expected, the head gradients show also a wider spread with increasing variance (Figs. 4g-i); the same holds true for power in the total downstream fluid flow. For simulations driven with a head difference ΔH = 10 m, the correlation relation between downstream power and the local head gradient was even stronger with values of r = 0.97, 0.94 and 0.91 for σ^2 =1, 3, and 5, respectively.

To check the inverse-linear relationship between ln(P) and ln(K), which was derived for the one-dimensional approximation as well (recall Eqs. 11 - 13), we related ln(P^x_{int}) for ΔH = 100 m to the logarithm of laterally averaged conductivity ln(K_{eff}) (Figs. 4 j-l). For the unit variance, we observe an almost perfect linear increase of ln(P^x_{int}) with a decline in ln(K_{eff}), as underpinned by the correlation coefficient of r = -0.92. This negative correlation declined with increasing

variance to values of r = -0.81 and r = -0.72 for σ^2 = 3 and σ^2 = 5, respectively, yet they are still significant. For the lower head of ΔH = 10 m, the anti-correlation is again stronger, with r values of -0.93, -0.83 and -0.76, for σ^2 =1, 3, and 5, respectively.

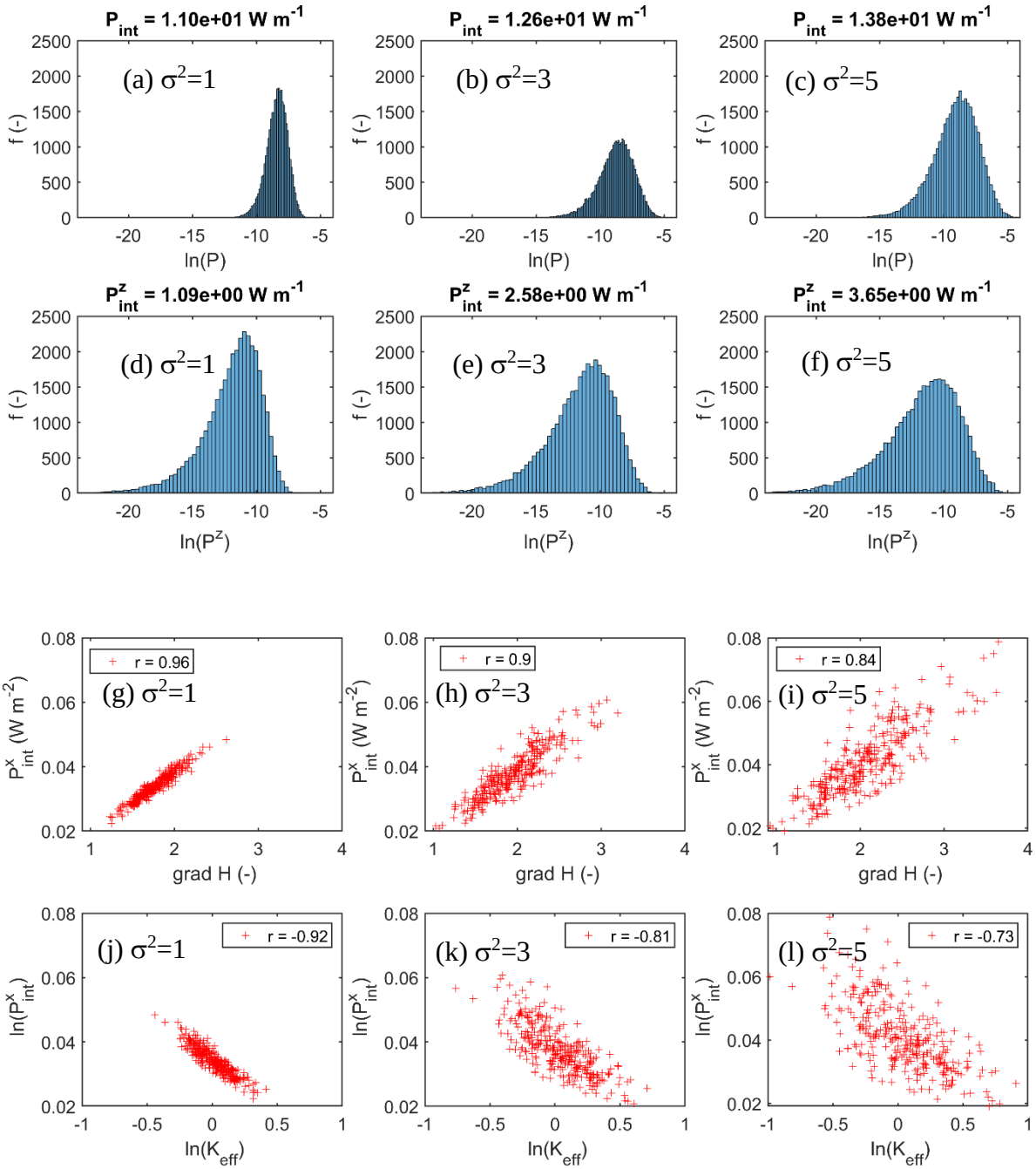

Figure 4. Histogram of log power ln(P) (**(a)**, **(b)**, **(c)**) and log power in the vertical water flux ln(P^z) ((e), (f) (g)) as function of the variance σ^2. Integral power P^x_{int} in the total downstream water flux, plotted against the laterally averaged head gradient (**(g)**, **(h)**, **(i)**), and ln(P^x_{int}) as function of the log of the transversally averaged K, ln(K_{eff}) (**(j)**, **(k)**, **(l)**).

We hence state that the system behaves energetically also in the case of the highest variance, largely similar to a heterogeneous one-dimensional system; this holds even truer in case of a smaller driving head difference. The power required to maintain the driving head difference and fluid flow in steady state increases, with increasing variance of the hydraulic conductivity field. Regions of high total power coincide with large positive deviations of the hydraulic head from its mean, which emerge in the vicinity of "bottlenecks" of low hydraulic conductivity. However, it is the increasing power in the vertical/transversal flow component that matters, as detailed in the next section.

4.3 Entropy as function of work and power along solute transport trajectories and

Figure 5 presents boxplots of the power in the vertical flow component P^z as function of the variance in ln(K) for the head differences of ΔH =100 m and 10 m. These results confirm that it is indeed mainly the power in the vertical flow component that grows with increasing variance of K. This makes intuitive sense, because transversal concentrations gradients are formed by vertical flow and transport of solute particles.

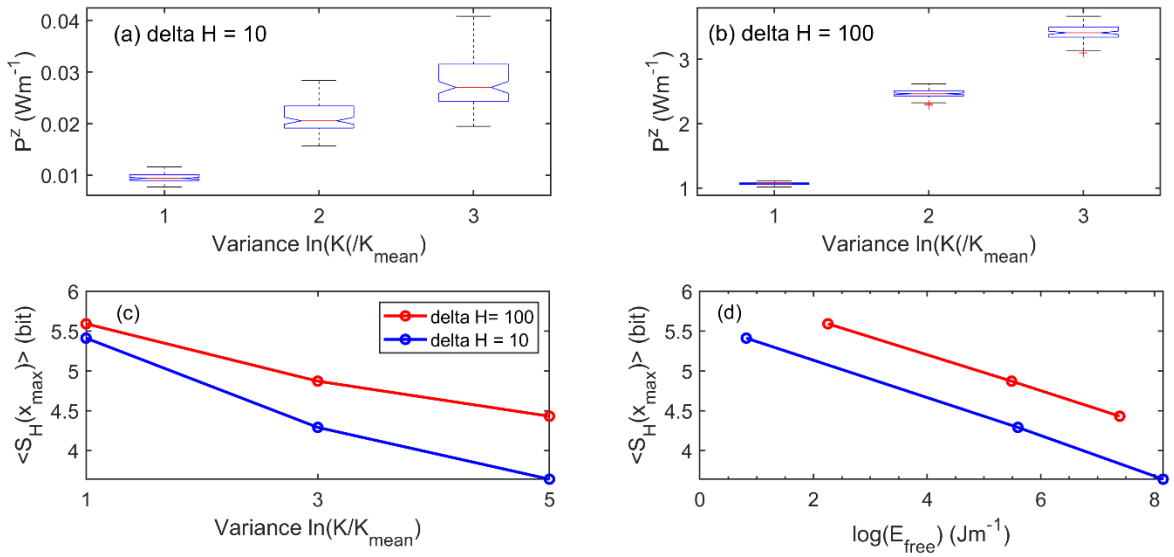

Figure 5. Boxplots of the power in the vertical flow component P^z as a function of the variance in ln(K) for the head difference **(a)** ΔH =100 m, and **(b)** ΔH = 10 m. The corresponding median flow path entropy of the ensembles at the domain outlet is plotted as a function of the variance of ln(K) (c) and against the median work E_{free} performed by the fluid. The latter is power times the maximum travel time to the outlet.

The growing power in the vertical flow component explains, hence, the stronger self-organization and declining flow path entropy with growing variance.

While the differences in vertical power P^z are significant between the variance cases, vertical power is in case of the ΔH = 10 m two orders of magnitude smaller than for the case of ΔH = 100 m. This is plausible as both the Darcy flow velocities and the local head gradients are on average 10 times smaller. The decline of the median entropy med($S_H(x_{max})$) with the med$<P^Z>$ reveals, in line with the gas laser example given in the Introduction, that a larger power input due to a higher pumping rate leads to an higher order in the macroscale preferential transport pattern. Yet the reduction in flow path entropy at the domain outlet is stronger with increasing variance for ΔH =10 m than for ΔH = 100 m (Fig. 5 c). This is nevertheless plausible because the particle travel times in the case of ΔH = 10 m are between a factor of 10 to 100 larger (see also Fig. 7). Hence, this extra residence time (a) compensates for the on-average 10 times smaller vertical flow velocities, and it (b) also implies that the work, defined as the integral of power in vertical flow along the particle travel times to the outlet, is larger for σ^2 = 3 and 5, as in case of ΔH = 100 (Fig 5 d). The larger amount of work performed by the vertical flow component explains well the stronger self-organization in the case of the lower head difference.

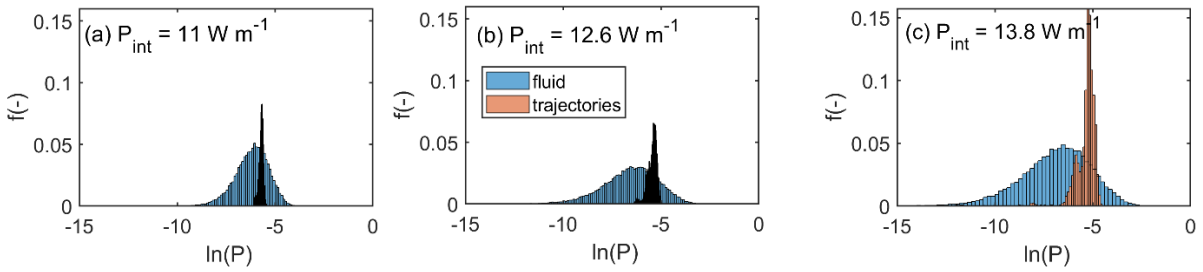

Figure 6: Cumulative distributions of ln(P) in the flow domain (blue) and of ln(P) averaged along the particle trajectories for **(a)** σ^2 = 1, **(b)** σ^2 = 3, and **(c)** σ^2 = 5.

Figure 6a, b, c compare the probability density distributions (pdfs) of ln(P) within the entire flow domain (blue), against the power averaged along the actual particle trajectories (in brown). While in the case of perfectly mixed flow and transport, both pdfs should be rather similar, they actually are remarkably different. This is because particles accumulate downstream along pathways of high vertical power into preferential pathways, and this is clearly reflected by the shift of the pdf's towards higher power values.

4.4 Space-time asymmetry and entropy export into the breakthough

To switch the observation perspective, we determined the particle breakthrough curves (BTC) for the different variances cases for and calculated their Shannon entropy as means of uncertainty and order in the arrival times, using the time step width of 0.1 dimensionless time units as bin width. For the head difference ΔH =100, the width of the breakthrough curves clearly increases with increasing variance, indicating an earlier breakthrough, a longer tailing and a more even distribution of normalized concentrations in time (Fig.7a). In the case ΔH =10, we observe a similar behavior, but a stronger and clear shift to larger breakthrough times, due to the smaller Darcy velocities (Fig. 7b). For both head differences one can observe that the Shannon entropy in arrival times grows with increasing variance of ln(K) reflecting a larger uncertainty and a declining order in the temporal distribution of travel times. In this context, it is important to recall that entropy cannot be consumed, due to the second law. This that means that the declining flow path entropy needs to be exported from the system.

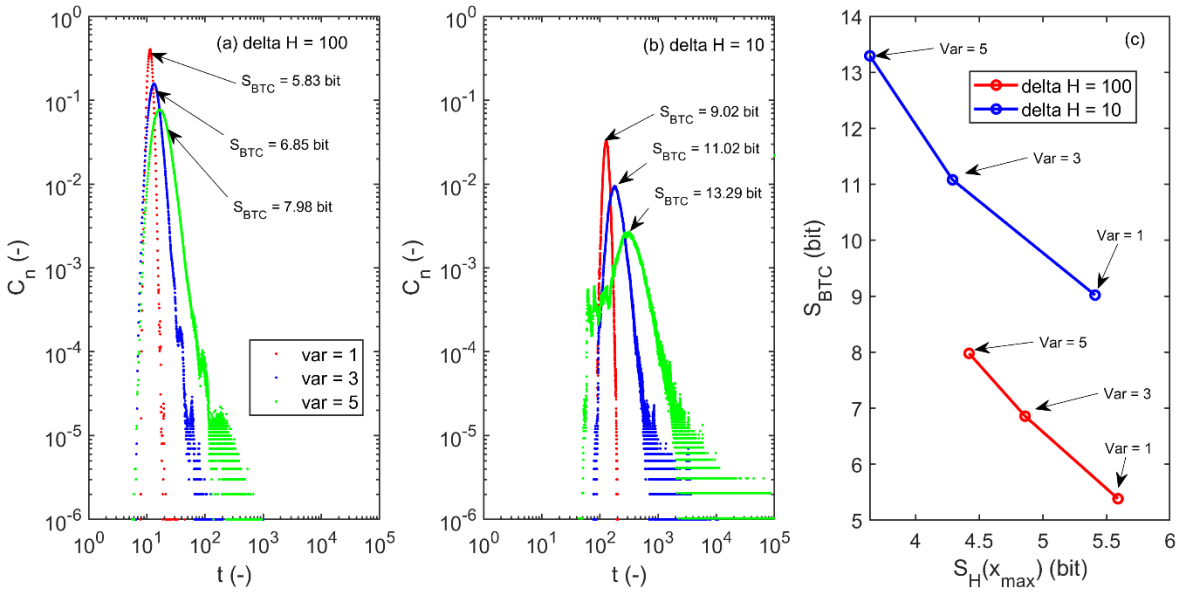

Figure 7. Breakthrough curves and their Shannon entropies S_{BTC} for **(a)** ΔH =100, and **(b)** ΔH =10; **(c)** S_{BTC} plotted against the flow path entropy of the downstream outlet $S_H(x_{max})$, before particles leave the domain, for all variance cases, and ΔH =100 and 10 respectively.

Figure 7b clearly visualizes this space-time asymmetry in entropies, the growing spatial organization with increasing variance of ln(K) translates due to the associated entropy export into a declining organization in arrival times. Please note that due to the different binning in

space and time, changes in S_{BTC} and S_H with changing variance cannot be exactly the same. In fact, also the entropy, which is produced due to energy dissipation. The opposite of the Shannon entropy monotonies corroborate nevertheless that reduced flow path entropy is indeed exported into the BTC.

5 Discussion

5.1 An energy and entropy centered framework to characterize and explain preferential flow

This study proposes an alternative framework to quantify and explain the enigmatic emergence of preferential flow and transport in heterogeneous saturated porous media, using concepts from thermodynamics and information theory. We examined simulations of two-dimensional fluid flow and solute transport based on the methods of Edery et al. (2014) at total head differences of 100 and 10 characterized the discrete probability distribution of solute particles to cross a distinct transversal position in a plane normal to the direction of the mean flow by means of the Shannon entropy. In general, we found a declining entropy with increasing downstream transport distance, reflecting a growing downstream self-organization due to the increasing concentration of particles in preferential flow paths. Strikingly, preferential flow patterns with lower entropies emerged when analyzing simulations in media with larger variances in hydraulic conductivity, and this enhanced self-organization appeared even stronger for simulations at lower head differences. This implies that macro-states of higher order are established, despite the higher randomness of ln(K) for a range of Peclet numbers representing strong and intermediate importance of advective transport. The key to explain this almost paradoxical behavior is the finding that power in the vertical flow components grows with the variance of the hydraulic conductivity field. Due to this larger energy input, the vertical/transversal flow component may perform more work to increase the order in the flow path distribution, through steepening transversal concentration gradients as reflected in lower entropies.

Notwithstanding these findings, we of course recognize that the concepts of entropy, free energy and work are, per se, not new in hydrology. We thus place our findings in context relative to related studies, in the sections below.

600 **5.2 Measuring irreversibility and macroscale organization using the Shannon entropy**

601 Here we show that the Shannon entropy of the transversal distribution of solutes is suited to
602 quantify the downstream emergence of preferential solute movement, as reflected in a declining
603 "flow path entropy". Lower flow path entropies and thus a stronger spatial order in preferential
604 transport are established when solutes are transported through stronger heterogeneous hydraulic
605 conductivity fields. In this context, we recall that Edery et al. (2014) analyzed breakthrough
606 curves using the continuous time domain random walk framework (Berkowitz et al., 2006).
607 When fitting an inverse power law to the breakthrough curves, the corresponding ß parameter
608 (which is a measure of the degree of anomalous transport, with ß increasing to 2 indicating
609 Fickian transport) increased with increasing variance of ln(K). Here we analyzed the Shannon
610 entropy of the breakthrough curves in time, and contrary to the flow path entropies, they grow
611 with increasing variance of ln(K). This means that higher degrees in spatial order in solute
612 transport that emerges at larger variances in ln(K), expressed by lower flow path entropies,
613 translate into a higher entropy and thus a higher disorder and thus uncertainty in arrival times.
614 This is reflected by an earlier first breakthrough, a retarded appearance of the peak
615 concentration, and a longer tailing in the breakthrough curves and higher similarity of the BTC
616 to a uniform, rectangular pulse. This finding coincides well with the illustrative case that
617 Bianchi and Pedretti (2017) used to compare solute breakthrough through ordered and
618 disordered alluvial aquifers.

619 This space-time asymmetry in entropy and organization can, however, only be explained using
620 the physical perspective of entropy and the second law. The emergence of spatially organized
621 preferential transport and the related decline in flow path entropy essentially requires an export
622 of the entropy from the system into the BTC. We thus conclude that the ß parameter of the
623 CTRW framework, is also two-fold measure for spatial organization of solute transport through
624 the system and temporal organization in arrival times and their asymmetry. One might hence
625 wonder whether a perfect spatial organization due to preferential transport of the entire solute
626 particles through a single preferential flow path would, in the case of a step input, translate into
627 a BTC of maximum entropy/disorder, i.e., rectangular BTC (and vice versa). We return to this
628 issue in Sect. 6.

629 We speculate, too, that the concepts of entropy, power and work might be helpful to explore
630 the interplay of dissolution and precipitation of minerals such as silicate or carbonate rock, and

631 the related local feedbacks on saturated hydraulic conductivity, as investigated by Edery et al.
632 (in review 2021). These processes certainly affect and change the distribution of entropy and
633 power in fluid flow. The key to assess this is to include molar entropy and the free energy
634 differences associated with the chemical reactions and chemical energy fluxes associated with
635 chemical transport into the entropy and energy balances.

636 **5.3 Preferred flow and transport pathways as maximum power structures?**

637 The idea that preferential flow coincides with a larger power in fluid flow has been discussed
638 widely in hydrology. Howard (1971, cited in Howard, 1990) proposed that angles of river
639 junctions are arranged in such way that they minimize stream power; later he postulated that
640 the topology of river networks reflects an energetic optimum, formulated as a minimum in total
641 energy dissipation in the network (Howard, 1990). This work inspired Rinaldo et al. (1996) to
642 propose the concept of minimum energy expenditure as an enslavement principle for the self-
643 organized development of river networks. Hergarten et al. (2014) transferred this concept to
644 groundwater systems. They derived preferential flow paths that minimize the total energy
645 dissipation at a given recharge, under the constraint of a given total porosity and showed that
646 these setups allowed predictions of spring discharge at several locations. Minimum energy
647 expenditure in the river network implies that power therein is maximized. In this light, Kleidon
648 et al. (2013) showed that directed structural growth in the topology of connected river networks
649 can be explained through a maximization of kinetic energy transfer to transported suspended
650 sediments.

651 Our findings are in line with but step beyond these studies, which commonly refer to
652 preferential flow in connected, highly conductive networks. Here we find that solute particles
653 prefer to move through pathways of very high vertical power, even when they are not connected
654 by a continuous set of cells of relatively high hydraulic conductivity. On the contrary, these
655 pathways incorporate regions of low hydraulic conductivity. This finding reflects the squared
656 dependence of power on the spatial head gradient, which in turn becomes largest in regions of
657 low hydraulic conductivity. We stress that this result, and our finding that a larger power input
658 (due to a higher pumping rate) leads to a higher order in the macroscale preferential transport
659 pattern, is a consequence of the imposed boundary condition. A steady-state head difference
660 implies a positive energetic feedback: in a real-world experiment, the pump provides this
661 feedback, as otherwise the gradient is depleted by the flowing fluid. Although such a positive

662 feedback is straightforwardly established in a numerical model by assigning the desired
663 constant head difference, it is important that this choice implies that such a positive feedback
664 exists. Due to this virtual energy input, the vertical flow component and solutes may perform
665 the necessary work to steepen the transversal concentrations and thereby establish an ordered
666 preferential flow pattern at the macroscale. Ultimately, it is the higher necessary pumping
667 rate/power and the duration of the experiment that determine the elevated total energy input
668 into the domains with higher K variance. This constrains the amount of work performed by
669 vertical flow components and explains (a) why preferential flow patterns of higher order emerge
670 with growing subscale randomness, and (b) why self-organization was even stronger in the case
671 of a lower driving head difference of 10.

672 One might hence wonder whether an even stronger self-organization might be observed during
673 similar simulations in 3D stochastic media. We generally expect similar behavior, because the
674 local changes in power of the transversal flow component arise from the local feedback on the
675 pressure head gradient upstream of the low conductivity bottlenecks. The gradients steepen
676 ahead of these bottlenecks, which implies a higher power in the transversal flow component.
677 This feedback will also occur in a 3D confined system, as it is a direct result of the boundary
678 conditions (no flow boundary conditions for the upper, lower, inlet and outlet boundaries).

679 **6 Conclusions and outlook**

680 Based on the presented findings, we conclude that the combined use of free energy and entropy
681 holds the key to characterize and quantify the self-organized emergence of preferential flow
682 phenomena and to explain the underlying cause of their emergence. Information entropy is an
683 excellent, straightforward concept to diagnose self-organization in space and time: Here, the
684 formation of preferential transport is reflected in the downstream decline in the entropy of the
685 transversal flow path distribution and that this decline becomes stronger with increasing
686 variance of hydraulic conductivity. The concepts of free energy and physical entropy, however,
687 provide the underlying cause: steepening of transversal concentration gradients requires work,
688 the formation of even steeper gradients and lower flow path entropies needs even more work
689 and thus a higher free energy input into the open system. The higher necessary pumping rate
690 and energy input into the domains is the reason, why spatial organization in preferential solute

691 movement increased with growing subscale randomness of hydraulic conductivity. This is
692 behavior is very much in line with what we discussed for the gas laser in the introduction.

693 Entropy can, however, due to the second law not be consumed, and the declining flow path
694 entropy is in fact be exported from the system into the breakthrough curve. Shannon entropy
695 allows again for the straightforward diagnosis, while physical entropy provides the reason for
696 this space-time asymmetry in entropy, organization and uncertainty. Transport of all solute
697 particles through a single preferential flow paths implied a maximum spatial organization and
698 maximum/knowledge certainty about the transversal spreading of solute. However, this would,
699 due to the entropy export, into a maximum disorder of and thus uncertainty about the arrival
700 times, as the BTC would correspond to rectangular pulse of uniform concentration. Advective
701 diffusive transport through a homogeneous flow field implied, in case of a spatially
702 homogeneous step input, maximum uncertainty about transversal position of solute molecules,
703 while the BTC would be perfectly certain and providing minimum uncertainty about arrival
704 times. This space-time asymmetry in entropy implies that perfect organization and certainty
705 about both flow paths and travel times can never simultaneously occur. This required
706 consummation of entropy and thus violation of the second law of thermodynamics. However,
707 we wonder whether effective predictions of the entropies in the BTC and the flow path
708 distributions based on the knowledge driving head differences and the variance and correlation
709 lengths of hydraulic conductivity might be achievable in the future. This will of course not tell
710 us where solutes move and when they breakthrough, but predict the related uncertainty as an
711 important constraint of transversal distribution of transport pathways and travel times.

712 **Acknowledgments**

713 E.Z. gratefully acknowledges intellectual support by the "Catchments as Organized Systems"
714 (CAOS) research unit and funding of the German Research Foundation, DFG, (FOR 1598, ZE
715 533/11-1, ZE 533/12-1). Y.E. thanks the support of the Israel Science Foundation (grant No.
716 801/20); B.B. thanks the support of the Israel Science Foundation (grant No. 1008/20) and the
717 Crystal Family Foundation. B.B. holds the Sam Zuckerberg Professorial Chair in Hydrology.
718 The authors acknowledge support by Deutsche Forschungsgemeinschaft and the Open Access
719 Publishing Fund of Karlsruhe Institute of Technology (KIT). The service charges for this open
720 access publication have been covered by a Research Centre of the Helmholtz Association.

We acknowledge the reviewers Danièle Pedretti and Hubert Savenije, and the editor Monica Rica for their thoughtful assessment of our work.

References

Ababou, R., D. McLaughlin, L. W. Gelhar, and A. F. B. Tompson: Numerical simulation of three-dimensional saturated flow in randomly heterogeneous porous media, Transp. Porous Media, 4, 549–565, 1989.

Applebaum, D. (1996). Probability and Information (First). Cambridge University Press.

Becker, M.W. and A.M. Shapiro: Tracer transport in fractured crystalline rock: Evidence of nondiffusive breakthrough tailing, Water Resources Research, 36(7), 1677-1686, 2000.

Ben-Naim: A., A Farewell to Entropy. World Scientific. Chapter 1, https://doi.org/10.1142/6469, 2008.

Berkowitz, B., and Zehe, E.: Surface water and groundwater: unifying conceptualization and quantification of the two "water worlds", Hydrology and Earth System Sciences, 24, 1831-1858, 10.5194/hess-24-1831-2020, 2020.

Berkowitz B. and Scher H.: Anomalous transport in correlated velocity fields, Physical Review E. 81, 1, 11128, 2010.

Berkowitz, B., A. Cortis, M. Dentz, and H. Scher: Modeling non-Fickian transport in geological formations as a continuous time random walk, Rev. Geophys., 44, RG2003, doi:10.1029, 2006.

Berkowitz B.: Characterizing flow and transport in fractured geological media: A review, Advances in Water Resources. 25(8-12), 861-884, 2002.

Beven, K., and Germann, P.: Water-Flow In Soil Macropores .2. A Combined Flow Model, Journal Of Soil Science, 32, 15-29, 1981.

Beven, K., and Germann, P.: Macropores And Water-Flow In Soils, Water Resources Research, 18, 1311-1325, 1982.

Bianchi, M., C. Zheng, C. Wilson, G. R. Tick, G. Liu, and S. M. Gorelick: Spatial connectivity in a highly heterogeneous aquifer: From cores to preferential flow paths, Water Resour. Res., 47, W05524, doi:10.1029/2009WR008966.

Bianchi, M., and Pedretti, D.: Geological entropy and solute transport in heterogeneous porous media, Water Resources Research, 53, 4691-4708, 10.1002/2016wr020195, 2017.

Bianchi, M., and Pedretti, D.: An entrogram-based approach to describe spatial heterogeneity with applications to solute transport in porous media, Water Resour. Res., 54, 4432-4448, 10.1029/2018wr022827, 2018.

Bolt, G. H., and M. J. Frissel: Thermodynamics of soil moisture, Netherlands journal of agricultural science, 8, 57-78.1960.

Chiogna, G., and Rolle, M.: Entropy-based critical reaction time for mixing-controlled reactive transport, Water Resources Research, 53, 7488-7498, 10.1002/2017wr020522, 2017.

Cirpka, O.A. and P.K. Kitanidis: Characterization of mixing and dilution in heterogeneous aquifers by means of local temporal moments, Water Resources Research, 36(5), 1221-1236, 2000.

Clausius, R.: Über die Art der Bewegung, welche wir Wärme nennen, Annalen der Physik und Chemie 79, p. 353 – 380, 1857.

de Dreuzy, J.-R., J. Carrera, M. Dentz, and T. Le Borgne:Time evolution of mixing in heterogeneous porous media, Water Resour. Res., 48, W06511, doi:10.1029/2011WR011360, 2012.

Dell'Oca, A., A. Guadagnini, and M. Riva: Interpretation of multi-scale permeability data through an information theory perspective, Hydrology and Earth System Sciences, 24(6), 3097-3109, 2020.

Domenico, P. A., and F. W. Schwartz: Physical and Chemical Hydrogeology, John Wiley, New York, 1990.

Edery, Y., Guadagnini, A., Scher, H., and Berkowitz, B.: Origins of anomalous transport in disordered media: Structural and dynamic controls, Water Resour. Res., 50, 1490-1505, doi:10.1002/2013WR015111, 2014.

Edery, Y., Stolar, M., Porta, G., and Guadagnini, A.: Feedback mechanisms between precipitation and dissolution reactions across randomly heterogeneous conductivity fields, Hydrol. Earth Syst. Sci. Discuss. [preprint], https://doi.org/10.5194/hess-2021-238, in review, 2021.

Fahle, M., Hohenbrink, T. L., Dietrich, O., and Lischeid, G.: Temporal variability of the optimal monitoring setup assessed using information theory, Water Resources Research, 51, 7723-7743, 10.1002/2015wr017137, 2015.

Fiori, A. and Jankovic, I.: On Preferential Flow, Channeling and Connectivity in Heterogeneous Porous Formations. Math Geosci 44, 133–145. https://doi.org/10.1007/s11004-011-9365-2, 2012.

Flury, M., Flühler, H., Leuenberger, J., and Jury, W. A.: Susceptibility of soils to preferential flow of water: a field study, Water resources research, 30, 1945-1954, 1994.

Groves, C. G., & Howard, A. D.: Early development of karst systems: 1. Preferential flow path enlargement under laminar flow. Water Resources Research, 30(10), 2837–2846. https://doi.org/10.1029/94WR01303, 1994.

Gómez-Hernánez, J. J., Sahuquillo, A., and Capilla, J.: Stochastic simulation of transmissivity fields conditional to both transmissivity and piezometric data—I. Theory, Journal of Hydrology, 203, 162-174, https://doi.org/10.1016/S0022-1694(97)00098-X, 1997.

Haken, H., *Synergetics: An Introduction; Nonequilibrium Phase Transitions and Self-organization in Physics, Chemistry and Biology* 355 p pp., Springer Berlin, 1983.

Jackisch, C., L. Angermann, N. Allroggen, M. Sprenger, T. Blume, J. Tronicke, and E. Zehe. Form and function in hillslope hydrology: in situ imaging and characterization of flow-relevant structures, Hydrology and Earth System Sciences, 21(7), 3749-3775, 2017.

Jaynes, E. T.: Information Theory and Statistical Mechanics, Phys. Rev. 106, 620, 1957.

Guadagnini, A., and S. P. Neuman: Nonlocal and localized analyses of conditional mean steady state flow in bounded, randomly nonuniform domains, 1, theory and computational approach, Water Resour. Res., 35, 2999–3018, 1999.

Hergarten, S., G. Winkler, and S. Birk: Transferring the concept of minimum energy dissipation from river networks to subsurface flow patterns, *Hydrology And Earth System Sciences*, *18*(10), 4277-4288, .2014.

Howard, A. D.: Theoretical model of optimal drainage networks, Water Resour. Res., 26, 2107-2117, 1990.

Klaus, J., and E. Zehe (2011), A novel explicit approach to model bromide and pesticide transport in connected soil structures, Hydrology And Earth System Sciences, 15(7), 2127-2144.

Kleidon, A. (2016), Thermodynamic foundations of the Earth system. New York NY: Cambridge University Press.

Kleidon, A., Zehe, E., Ehret, U., and Scherer, U.: Thermodynamics, maximum power, and the dynamics of preferential river flow structures at the continental scale, Hydrology And Earth System Sciences, 17, 225-251, 10.5194/hess-17-225-2013, 2013.
Kleidon, A., Renner, M., and Porada, P.: Estimates of the climatological land surface energy and water balance derived from maximum convective power, Hydrology And Earth System Sciences, 18, 2201-2218, 10.5194/hess-18-2201-2014, 2014.
Kitanidis, P.K.: The concept of the Dilution Index, Water Resources Research, 30(7), 2011-2026. https://doi.org/10.1029/94WR00762, 1994.
Kondepudi, D., and Prigogine, I.: Modern Thermodynamics: From Heat Engines to Dissipative Structures, John Wiley Chichester, U. K., 1998.
LaBolle, E.M. and G.E. Fogg: Role of molecular diffusion in contaminant migration and recovery in an alluvial aquifer system, Transport in Porous Media 42: 155–179, 2001.
Levy, M., and B. Berkowitz: Measurement and analysis of non-Fickian dispersion in heterogeneous porous media, J. Contam. Hydrol., 64, 203–226, 2003.
Loritz, R., Hrachowitz, M., Neuper, M., and E. Zehe: The role and value of distributed precipitation data in hydrological models, Hydrol. Earth Syst. Sci., 25, 147–167., https://doi.org/10.5194/hess-25-147-2021,2021,
Loritz, R., Gupta, H., Jackisch, C., Westhoff, M., Kleidon, A., Ehret, U., and Zehe, E.: On the dynamic nature of hydrological similarity, Hydrology And Earth System Sciences, 22, 3663-3684, 10.5194/hess-22-3663-2018, 2018.
Loritz, R., Kleidon, A., Jackisch, C., Westhoff, M., Ehret, U., Gupta, H., and Zehe, E.: A topographic index explaining hydrological similarity by accounting for the joint controls of runoff formation, Hydrology And Earth System Sciences, 23, 3807-3821, 10.5194/hess-23-3807-2019, 2019.
Lotka, A. J.: Contribution to the energetics of evolution, Proc Natl Acad Sci USA, 8, 147-151, 1922a.
Lotka, A. J.: Natural selection as a physical principle, Proc Natl Acad Sci USA, 8, 151-154, 1922b.
Malicke, M., Hassler, S. K., Blume, T., Weiler, M., and Zehe, E.: Soil moisture: variable in space but redundant in time, Hydrology and Earth System Sciences, 24, 2633-2653, 10.5194/hess-24-2633-2020, 2020.
Morvillo, M., Bonazzi, A., Rizzo, C.B.:. Improving the computational efficiency of first arrival time uncertainty estimation using a connectivity-based ranking Monte Carlo method. Stoch Environ Res Risk Assess. https://doi.org/10.1007/s00477-020-01943-5, 2021.
Nowak, W., Y. Rubin, and F. P. J. de Barros: A hypothesis-driven approach to optimize field campaigns, *Water Resources Research*, *48*, Nowak, W., Rubin, Y., and de Barros, F. P. J.: A hypothesis-driven approach to optimize field campaigns, Water Resources Research, 48, 10.1029/2011wr011016, 2012.
Paltridge, G. W.: CLIMATE AND THERMODYNAMIC SYSTEMS OF MAXIMUM DISSIPATION, Nature, 279, 630-631, 10.1038/279630a0, 1979.
Rinaldo, A., Maritan, A., Colaiori, F., Flammini, A., and Rigon, R.: Thermodynamics of fractal networks, Physical Review Letters, 76, 3364-3367, 1996.
Riva, M., A. Guadagnini, and X. Sanchez-Vila: Effect of sorption heterogeneity on moments of solute residence time in convergent flows, Math. Geosci., 41, 835–853, doi:10.1007/s11004-009-9240-6, 2009.
Shannon, C. E.: A Mathematical Theory Of Communication, *Bell System Technical Journal*, *27*(4), 623-656, 1948.

Sternagel, A., R. Loritz, W. Wilcke, and E. Zehe: Simulating preferential soil water flow and tracer transport using the Lagrangian Soil Water and Solute Transport Model, Hydrology And Earth System Sciences, 23(10), 4249-4267, 2019.

Sternagel, A., R. Loritz, J. Klaus, B. Berkowitz, and E. Zehe: Simulation of reactive solute transport in the critical zone: a Lagrangian model for transient flow and preferential transport, Hydrology and Earth System Sciences, 25(3), 1483-1508,(2021.

Schroers, S., Eiff, O., Kleidon, A., Wienhöfer, J., and Zehe, E.: Hortonian Overland Flow, Hillslope Morphology and Stream Power I: Spatial Energy Distributions and Steady-state Power Maxima, Hydrol. Earth Syst. Sci. Discuss. [preprint], https://doi.org/10.5194/hess-2021-79, in review, 2021.

Šimůnek, J., Jarvis, N. J., van Genuchten, M. T., and Gärdenäs, A.: Review and Comparison of models for describing non-equilibrium and preferential flow and transport in the vadose zone, Journal of Hydrology, 272, 14-35, 2003.

Tietjen, B., E. Zehe, and F. Jeltsch: Simulating plant water availability in dry lands under climate change: A generic model of two soil layers, Water Resources Research, 45. https://doi.org/10.1029/2007WR006589,(2009.

van Schaik, L., J. Palm, J. Klaus, E. Zehe, and B. Schroeder: Linking spatial earthworm distribution to macropore numbers and hydrological effectiveness, Ecohydrology, 7(2), 401-408, 2014.

Wienhofer, J., and E. Zehe: Predicting subsurface stormflow response of a forested hillslope - the role of connected flow paths, Hydrology And Earth System Sciences, 18(1), 121-138, 2014.

Wienhöfer, J., K. Germer, F. Lindenmaier, A. Färber, and E. Zehe: Applied tracers for the observation of subsurface stormflow on the hillslope scale, *Hydrology and Earth System Sciences*, *13*(1145-1161), 2009.

Willmann, M., J. Carrera and X. Sánchez-Vila: Transport upscaling in heterogeneous aquifers: What physical parameters control memory functions? Water Resources Research, 44, W12437, doi:10.1029/2007WR006531, 2008.

Woodbury A.D. and T. J. Ulrych: Minimum relative entropy: Forward probabilistic modeling, Water Resources Research, 29(8), 2847-2860, https://doi.org/10.1029/93WR00923, 1993.

Zehe, E., and Fluhler, H.: Preferential transport of isoproturon at a plot scale and a field scale tile-drained site, Journal of Hydrology, 247, 100-115, 2001.

Zehe, E., Blume, T., and Bloschl, G.: The principle of 'maximum energy dissipation': a novel thermodynamic perspective on rapid water flow in connected soil structures, Philos. Trans. R. Soc. B-Biol. Sci., 365, 1377-1386, 10.1098/rstb.2009.0308, 2010.

Zehe, E., Ehret, U., Blume, T., Kleidon, A., Scherer, U., and Westhoff, M.: A thermodynamic approach to link self-organization, preferential flow and rainfall-runoff behaviour, Hydrology And Earth System Sciences, 17, 4297-4322, 10.5194/hess-17-4297-2013, 2013.

Zehe, E., Loritz, R., Jackisch, C., Westhoff, M., Kleidon, A., Blume, T., Hassler, S. K., and Savenije, H. H.: Energy states of soil water - a thermodynamic perspective on soil water dynamics and storage-controlled streamflow, Hydrology And Earth System Sciences, 23, 971-987, 10.5194/hess-23-971-2019, 2019.